Journal of Nanoporous Systems

Original Research Paper

Mesoporous Core-Shell Nanostructure with Integrated Magnetic Functionality for the Adsorptive Removal of Diclofenac from Aqueous Solutions

Somayeh Zalani[1], Asiyeh Sheikhzadeh Takabi*[2], Fereshteh Abbasi[3]

[1]*Faculty of Natural Resources and Environment, Tehran Science and Research Branch, Islamic Azad University, Tehran, Iran.*
[2] *Department of Chemistry, Faculty of Science, Shahid Chamran University of Ahvaz, Ahvaz 61357-43311, Iran*
[3]*Department of Chemistry, Il.C., Islamic Azad University, Ilam, Iran*

Article history
Received: 5 November 2025
Revised: 25 January 2026
Accepted: 29 January 2026

*Corresponding Author:
Asiyeh Sheikhzadeh Takabi, Department of Chemistry, Faculty of Science, Shahid Chamran University of Ahvaz, Ahvaz 61357-43311, Iran.

Email:
a_sheikhzadeh88@yahoo.com

Abstract: Pharmaceutical pollutants such as Diclofenac (DCF) remain in aquatic environments, leading to risks for ecological and human health. This research introduces a novel nanoporous magnetic Fe_3O_4@Bi_2O_3 core-shell nanocomposite intended for effective DCF adsorption. The composite features a magnetic Fe_3O_4 core encased in a highly porous, flower-like Bi_2O_3 shell, ensuring easy separability and outstanding uptake capacity. Structural analyses, including SEM, TEM, XRD, FT-IR, and BET, verified the successful creation of a nanoporous material with a surface area of 11.19 $m^2 g^{-1}$. Batch adsorption tests assessed the influences of initial DCF concentration, adsorbent dosage, contact time, and pH values. Findings revealed that the nanocomposite demonstrated remarkable adsorption capability, attributed to its extensive surface area and the synergistic interactions of the core and shell. Maximum monolayer capacity was recorded at 84.7 mg g^{-1}, aligning with the Freundlich isotherm and following pseudo-second-order kinetics. The Fe_3O_4@Bi_2O_3 showed excellent reusability and significant promise for sustainable water treatment, with adsorption mechanisms driven by electrostatic interactions, π–π stacking, and pore-filling within the nanoporous.

Keywords: Adsorption, Diclofenac, Core-Shell Nanocomposite, Magnetic Separation, Water Treatment.

Introduction

The rising use of pharmaceuticals and their resultant discharge into aquatic ecosystems is increasingly seen as a significant global environmental concern. This category of "emerging contaminants" is particularly alarming due to its biological activity and persistence, often eluding traditional wastewater treatment methods [1]. A prominent case is Diclofenac (2-[2-(2,6-dichloranilino)phenyl]acetic acid), a widely-used non-steroidal anti-inflammatory drug (NSAID) that is frequently found in water bodies because of its extensive use and resistance to degradation [2]. Even trace levels (ng/L to µg/L) of this compound have been associated with dire ecological effects, including liver damage in fish, kidney failure in vultures, and disruption of microbial ecosystems [3, 4]. Moreover, the risks of bioaccumulation and chronic human health hazards through prolonged exposure via drinking water signal an urgent need for action [5]. Thus, developing efficient, scalable, and cost-effective methods to fully eliminate DCF is critically important.

Among the various remediation strategies, adsorption there is preferred for its straightforward implementation, high efficiency, resilience to toxic compositions, and potential for regeneration [6]. The effectiveness of this approach is closely tied to the creation of high-performance adsorbents. Recent advancements have centered on sophisticated nanoadsorbents with elevated surface-area-to-volume ratios and adjustable surface chemistries [7, 8]. In the present arena, core-shell nanostructures present a promising avenue by merging the benefits of diverse materials. A magnetic core, typically composed of Fe_3O_4 (magnetite), facilitates the easy and rapid extraction of the adsorbent from the treated solution using an external magnetic field, thereby addressing a major challenge in nanotechnology: the recovery of fine particles [9,10]. Additionally, a functional shell can be precisely designed to enhance specific surface area, enable tailored porosity, and provide active sites that optimize adsorption of target pollutants.

Bismuth oxide (Bi_2O_3) has gained attention not only in photocatalysis but also in adsorption, thanks to its non-toxic, cost-efficient qualities and unique electronic structure that enhances the interactions with organic compounds [11,12]. Its adaptability is further increased by its capacity to form various nanostructures. When synthesized into a three-dimensional, flower-like porous form, Bi_2O_3 can deliver an exceptionally high surface area, plentiful active sites, and interconnected pore networks conducive to the diffusion and capture of organic molecules like DCF [13,14]. However, the efficacy of pure Bi_2O_3 nanostructures is often limited by challenges in separation and recovery from suspension post-adsorption [15].

In this study, we introduce for the first time the strategic design and synthesis of a novel magnetic Fe_3O_4@Bi_2O_3 core-shell nanocomposite, featuring a flower-like porous Bi_2O_3 shell directly grown on a spherical Fe_3O_4 core. This structure is engineered to harness a synergistic effect, combining the remarkable magnetic separability of the Fe_3O_4 core with the enhanced adsorption capability provided by the high-surface-area, porous Bi_2O_3 shell. The nanocomposite was thoroughly characterized using a comprehensive array of analytical techniques, and its performance was systematically assessed for DCF removal from aqueous solutions under varying conditions, such as initial DCF concentration (3-20 mg/L), adsorbent dosage (0.1-0.5 g/L), contact time (0-180 min), and pH (3-9). The present study aims to present a new, efficient, and easily recoverable adsorbent to address pharmaceutical pollution in water.

Experimental Materials

Ferric chloride hexahydrate ($FeCl_3 \cdot 6H_2O$), ferrous sulfate heptahydrate ($FeSO_4 \cdot 7H_2O$), bismuth nitrate pentahydrate ($Bi(NO_3)_3 \cdot 5H_2O$), urea, ammonium hydroxide (NH_4OH, 25%), and diclofenac sodium were sourced from Sigma-Aldrich. All reagents were of analytical grade and utilized without any additional purification. Deionized (DI) water was employed for all experimental procedures. The morphologies of the synthesized samples were examined using scanning electron microscopy (SEM) and transmission electron microscopy (TEM). The crystal phases of the samples were investigated through X-ray diffraction (XRD) analysis with a radiation wavelength of (λ = 0.15418 nm). The powder XRD patterns were recorded at a scan rate of 0.11 s^{-1} over a 2θ range of 10–80°. Fourier transform infrared (FT-IR) spectra of the produced material were gathered at room temperature, using a 100 mg KBr pellet with 1 mg of the sample. Absorbance readings were conducted using a UV-Visible spectrophotometer (Cintra 101 GBC Scientific Equipment Ltd).

Synthesis of Nanoporous Fe_3O_4@Bi_2O_3

Synthesis of Magnetic Fe_3O_4 Core: Spherical Fe_3O_4 nanoparticles were created through a co-precipitation technique. In summary, a molar ratio of Fe^{2+} to Fe^{3+} (1:2) was dissolved in 100 mL of deionized water while maintaining a nitrogen atmosphere. The solution was heated to 80°C, followed by the gradual addition of 10 mL of NH_4OH under vigorous stirring. The resulting black precipitate was isolated using a magnet, repeatedly washed with deionized water and ethanol, and finally dried at 60°C for 12 hours [16].

Synthesis of Porous Bi_2O_3 Shell: The core-shell structure of Fe_3O_4@Bi_2O_3 was constructed using a hydrothermal method. A total of 0.5 g of the synthesized Fe_3O_4 nanoparticles was dispersed in 60 mL of deionized water through ultrasonication. Subsequently, 2 mmol of $Bi(NO_3)_3 \cdot 5H_2O$ and 6 mmol of urea were introduced into the suspension with constant stirring. This mixture was then placed in a 100 mL Teflon-lined stainless-steel

autoclave and heated at 160°C for 12 hours. The final product was retrieved magnetically, thoroughly washed, and calcined at 400°C for 2 hours to yield the crystalline, porous Fe_3O_4@Bi_2O_3 nanocomposite [17].

Investigation of Adsorbent Activity on Removal of DCF Solution

Batch adsorption experiments were performed by introducing a specific amount of the Fe_3O_4@Bi_2O_3 nanocomposite into 50 mL of DCF solution contained in 100 mL Erlenmeyer flasks. The flasks were stirred on an orbital shaker maintained at a steady temperature (25±1°C). Various parameters were examined: initial DCF concentration (3-20 mg/L), adsorbent dosage (0.1-0.5 g/L), contact time (0-180 min), and pH (3-9, regulated with phosphate buffer). Samples were collected at set time intervals, and the adsorbent was removed using a magnet. The residual DCF concentration in the supernatant was determined using a UV-Vis spectrophotometer at its peak absorbance wavelength of 276 nm. The percentage of DCF removal (Removal %) was calculated for each trial using Eq. 1:

$$\text{Removal}(\%) = \frac{(C_0 - C_e)}{C_0} \times 100 \quad (1)$$

The adsorption capacity at time t, q_t (mg/g), was calculated using the Eq. 2:

$$q_e = \frac{(C_0 - C_e)}{m} \times V \quad (2)$$

where C_0 and C_t (mg/L) are the initial and at-time DCF concentrations, respectively, V (L) is the volume of the solution, and m (g) is the mass of the adsorbent.

Results and discussion:

The X-ray diffraction (XRD) spectrum of the nanoporous Fe_3O_4@Bi_2O_3 composite is shown in Fig. 1. This spectrum affirms the successful synthesis of the composite, showcasing distinct peaks attributable to the Fe_3O_4 and Bi_2O_3 components. The identified peaks for Fe_3O_4 at 2θ = 8.57°, 4.53°, 1.43°, 5.35°, and 1.30° correspond to the (220), (311), (400), (422), and (511) crystallographic planes, respectively, in alignment with standard card 19-0629 [18]. Concurrently, the characteristic peaks for Bi_2O_3 appeared at 2θ = 4.46°, 3.33°, and 5.27°, linked to the (120), (121), and (041) planes, as well as additional peaks, confirming its presence according to standard card 41-1449. The XRD results confirmed the composite includes mixed crystalline phases of magnetite Fe_3O_4 and monoclinic Bi_2O_3 [19].

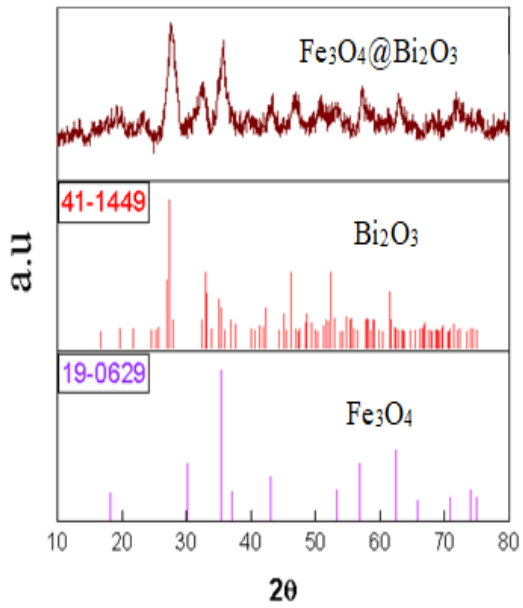

Fig. 1. The X-ray diffraction (XRD) pattern of the nanoporous Fe_3O_4@Bi_2O_3

The surface morphology of the synthesized samples was researched by SEM and TEM methods, as shown in Fig. 2. Figures 2a and 2b are the SEM and TEM images, respectively, of the bare Fe_3O_4 nanospheres. Figures 2c and 2d are the SEM and TEM images, respectively, of the final Fe_3O_4@Bi_2O_3 composite, revealing its distinctive flower-like porous architecture

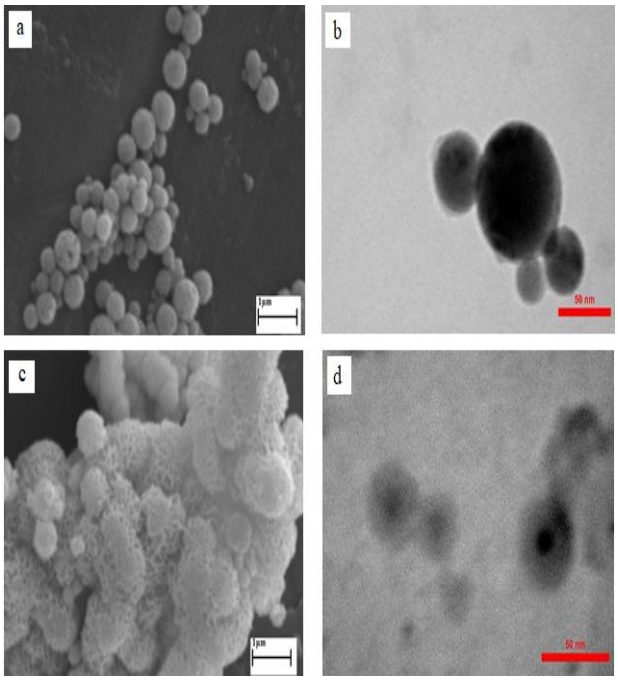

Fig. 2. SEM and TEM micrographs: (a) SEM and (b) TEM of Fe_3O_4 nanoparticles; (c) SEM and (d) TEM of the Fe_3O_4@Bi_2O_3 core-shell nanocomposite

FT-IR method is used to identify the type of bonds present in a compound. The spectrum of the Fe_3O_4@Bi_2O_3 composite (Fig. 3) confirms the successful integration of both materials. The strong absorptions at 3400-3300 cm^{-1} are attributed to the O–H stretching vibration of water molecules physically adsorbed on the high-surface-area nanomaterial. The peaks in the region of 560 cm^{-1} and 664 cm^{-1} are characteristic of the Fe–O vibrations from the magnetite core. Critically, the distinct peaks in the regions of 1393 cm^{-1} and 1843 cm^{-1} correspond to the Bi–O stretching vibrations, which are the definitive infrared fingerprints for bismuth oxide. The simultaneous presence of these Fe–O and Bi–O bands verifies the core–shell formation and strong interfacial binding [17, 20].

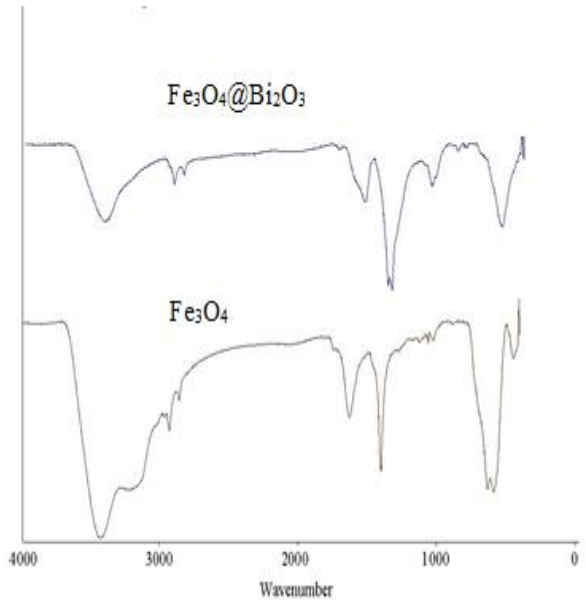

Fig. 3. FT-IR spectra for the nanocomposites.

Fig. 4. shows the absorption-desorption curve of nitrogen gas at a constant temperature on the surface of Fe_3O_4@ Bi_2O_3. BET analyses indicated a specific surface area of 11.19 m^2 g^{-1} characteristic of porous sorbents. From the BET analysis data, it can be noted that the total pore volume was obtained for the Fe_3O_4@ Bi_2O_3 structure to be 0.04908 cm^3 g^{-1}. The pore size distribution calculated using the BJH method and from the surface desorption curve is shown It can be concluded that the pore diameter of Fe_3O_4@Bi_2O_3 is in the range of 1–10 nm, which confirms its mesoporous nature according to the IUPAC classification (pores between 2–50 nm). The hysteresis loop corresponded to type-IV isotherms typical for mesoporous materials.

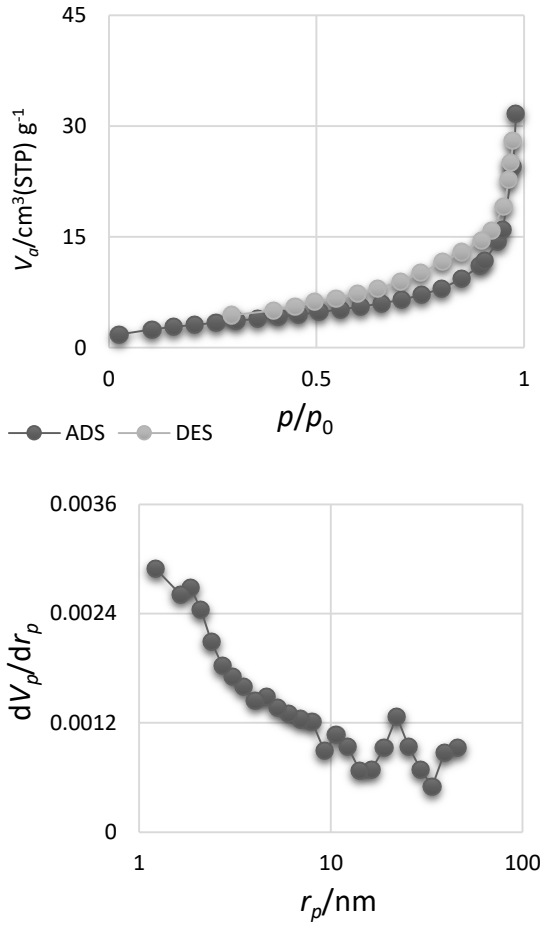

Fig. 4. The adsorption-desorption curve and distribution of the size of the pores for Fe_3O_4@Bi_2O_3

Adsorbent activity in the DCF removal

Initial DCF Concentration and Contact Time: The removal capacity (%) increased with an increase in the initial DCF concentration from 3 to 20 mg/L, due to a higher driving force for mass transfer. Equilibrium was reached within 120 minutes for all concentrations. The rapid initial adsorption rate can be attributed to the abundance of active sites on the porous shell (Fig. 5).

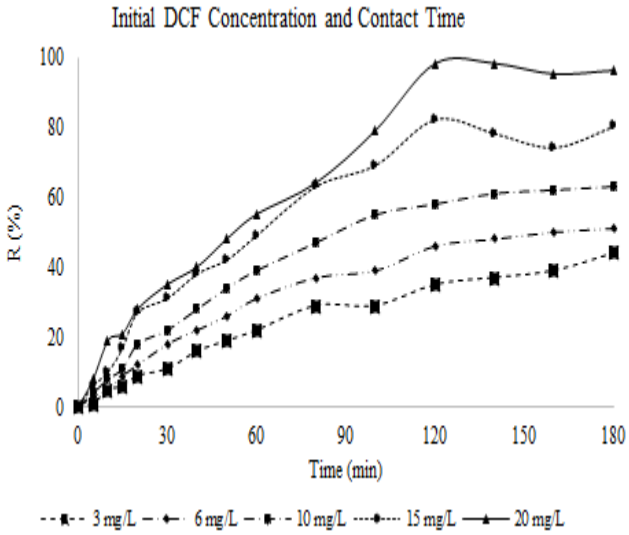

Fig. 5. Effect Initial Concentration on DCF removal percentage

Adsorbent Dosage: The removal efficiency of DCF increased from 45% to 98% as the adsorbent dosage increased from 0.1 to 0.5 g/L, owing to the increased surface area and availability of more adsorption sites. A further increase to 0.5 g/L only marginally improved removal, hence 0.5 g/L was selected as the optimum dosage. Increasing adsorbent dosage enhanced DCF removal, reaching 98% efficiency at 0.5 g/L. Adsorption equilibrium was achieved within 120 min, consistent with fast kinetics driven by high nanopore accessibility (Fig. 6).

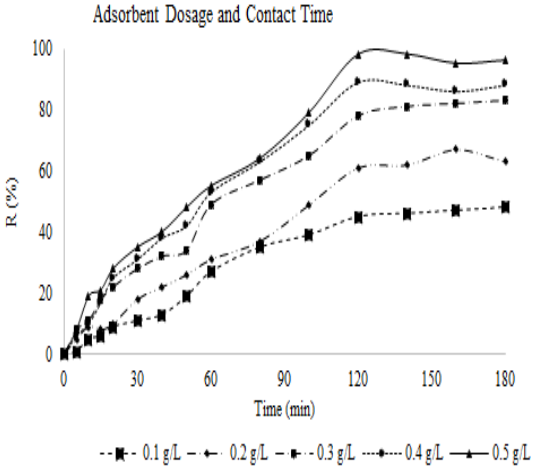

Fig. 6. Effect of adsorbent dose on DCF removal percentage

Effect of pH (Buffer): The pH of the solution significantly influenced on the adsorption process. The maximum DCF removal was observed at pH 5 (Fig. 7). Diclofenac (pKa ≈ 4.15) exists predominantly as anions (DCF^-) at pH > 4.15, while the surface of Bi_2O_3 can be protonated in acidic conditions. Therefore, at pH 5, strong electrostatic attraction occurs between the positively charged adsorbent surface and the anionic DCF molecules. At higher pH, the adsorbent surface becomes negatively charged, leading to electrostatic repulsion and a decrease in adsorption capacity. The maximum removal efficiency occurred at pH 5, where electrostatic attraction between protonated Bi_2O_3 surfaces and negatively charged DCF^- species was maximized [21,22]. At higher pH values (≥7), surface deprotonation led to decreased adsorption—behavior consistent with the point of zero charge (pH_pzc ≈ 6.2) for Bi_2O_3.

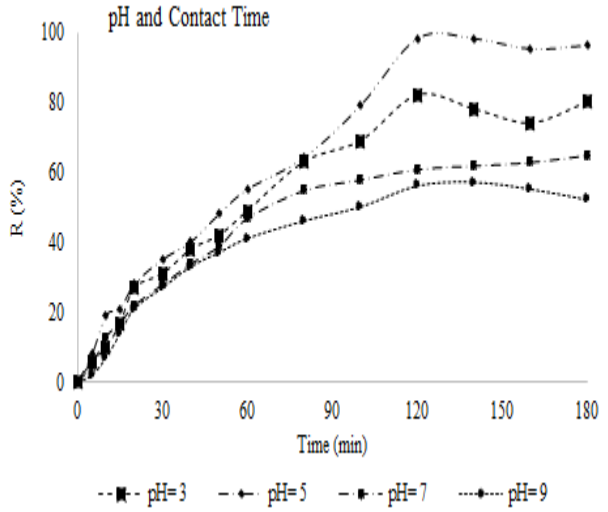

Fig. 7. Effect of pH on DCF removal percentage

Adsorption Isotherms and Kinetics

Adsorption isotherm describes the distribution of adsorbed molecules between the solid and liquid phases when the adsorption process reaches equilibrium. It is crucial to fit isotherm data to different models to identify a suitable model for design purposes. The Langmuir and Freundlich models are used to interpret the experimental data of liquid phase adsorption isotherms [23].

Langmuir's model is mathematically expressed as follows (Eq. 3):

$$\frac{C_e}{q_e} = \frac{1}{q_{max}b} + \frac{C_e}{q_{max}} \quad (3)$$

With Ce is the equilibrium concentration of the adsorbate (mg/l), qe is the amount of adsorbate adsorbed per unit of adsorbent (mg/g), q_{max} corresponds to Langmuir constants related to adsorption capacity, and b represents the rate of adsorption.

Freundlich's model is expressed as follows (Eq. 4):

$$\log q_e = \log k_F + \frac{1}{n}\log C_e \quad (4)$$

Here, q_e denotes the amount of adsorbate adsorbed per unit mass of adsorbent (mg/g), k_F and n are Freundlich constants, where n indicates the favorability of the adsorption process, and C_e is the equilibrium concentration of the adsorbate (mg/l).

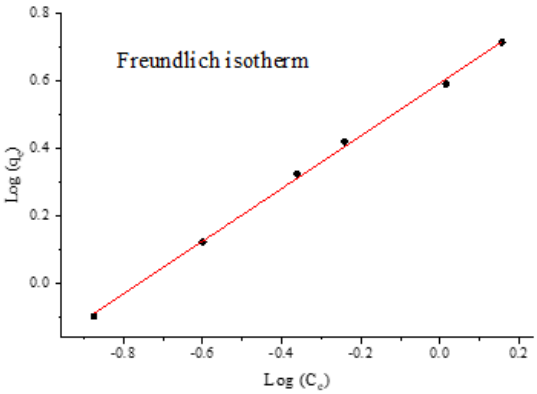

Fig. 8. Adsorption isotherms of DCF by Fe_3O_4@Bi_2O_3 (conditions: 20 mg/l of DCF, contact time: 180 min and 0.5 mg/g of Fe_3O_4@Bi_2O_3 at 25 °C).

The equilibrium data were analyzed using both the Langmuir and Freundlich isotherm models. The Freundlich model showed a superior fit (R^2 > 0.99), indicating that adsorption occurs in a monolayer on a uniform surface with energetically consistent nanoporous sites. The maximum monolayer adsorption capacity (q_{max}) was determined to be 84.7 mg/g, which is comparable to other adsorbents reported in the literature [5].

The investigation of DCF adsorption on Fe_3O_4@Bi_2O_3 was approached by applying pseudo-first-order and pseudo-second-order rate laws to accurately interpret the experimental findings [18], [20].

The pseudo-first-order kinetic model is expressed by the following Eq. 5:

$$q_t = q_e(1 - e^{-k_1 t}) \quad (5)$$

where qt and qe (mg/g) represent the amounts of sorbed DCF at time t and equilibrium, respectively, and k_1 (min^{-1}) is the first-order rate constant.
The pseudo-second-order kinetic is expressed by the following Eq. 6.

$$q_t = \frac{q_e^2 k_2 t}{1+q_e k_2 t} \quad (6)$$

Here, k_2 is the pseudo-second-order rate constant (g $mg^{-1}min^{-1}$).

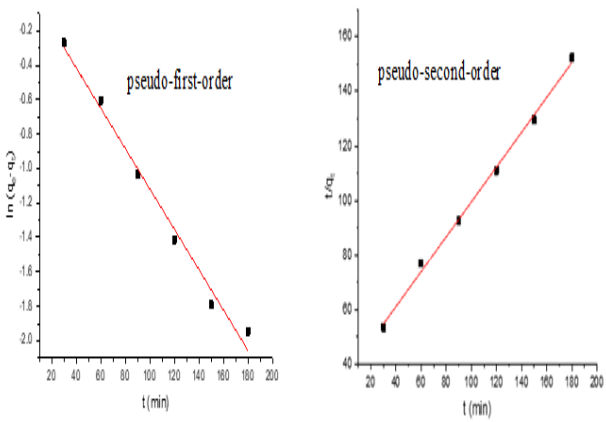

Fig. 9. Adsorption kinetics of DCF by Fe_3O_4@Bi_2O_3 (conditions: 20 mg/l of DCF, contact time: 180 min and 0.5 mg/g of Fe_3O_4@Bi_2O_3 at 25 °C).

The kinetic data were optimally represented by the pseudo-second-order model (R^2 > 0.99), suggesting that the adsorption mechanism is primarily driven by chemisorption, possibly involving valence forces through electron sharing or exchange between the adsorbent and DCF. This implies chemisorption entails electron transfer or hydrogen-bonding interactions between DCF and the surface functional groups. When compared with other adsorbents like Fe_3O_4@SiO_2, Fe_3O_4@ZnO, and MOF-based composites, this material exhibits competitive or even superior performance, which is attributed to its flower-like hierarchical nanoporous structure [24, 25].

Mechanism of Adsorption

The elimination of Diclofenac (DCF) is enhanced by a synergistic interplay of various adsorption mechanisms that focus on distinct molecular interactions:
Electrostatic Attraction: In the experimental setup, the adsorbent surface becomes protonated, resulting in the formation of Bi–OH_2^+ sites. These positively charged areas strongly attract the anionic DCF^- species present in the solution, thereby enabling effective initial capture.
π–π Stacking Interactions: The adsorption process gains further stability through π–π electron donor-acceptor interactions. The aromatic rings of the DCF molecule align with the electron-rich regions of the adsorbent surface, typically linked to oxygen orbitals (like those in Bi_2O_3), providing an additional, non-electrostatic binding energy contribution [22].
Nanoporous Confinement and Pore Filling: The nanoporous structure of the Bi_2O_3 shell is crucial for more than just surface area. When DCF molecules are adsorbed in pores smaller than 10 nm, the interaction of overlapping electric double layers and the closeness of the pore walls creates a nanoconfinement effect. This significantly boosts the strength of van der Waals interactions and raises the overall adsorption enthalpy, enhancing both capacity and selectivity for DCF uptake.
Magnetic Separation Capability: The composite configuration features an Fe_3O_4 core, delivering a strong magnetic response. This allows for the swift and effective separation of the adsorbent from the treated aqueous solution via an external magnetic field, ensuring that the integrity of the adsorbent is preserved while also enabling practical recovery post-treatment.

Discussion and Conclusion

This research successfully presented the development of a novel magnetic Fe_3O_4@Bi_2O_3 core-shell nanocomposite designed for the effective removal of diclofenac from water. The unique architecture, featuring a magnetic core combined with a flower-like, porous Bi_2O_3 shell, provides the adsorbent with multiple advantageous characteristics: (1) a large surface area and high porosity for abundant

adsorption sites, (2) excellent magnetic separability facilitating easy recovery and potential reusability, and (3) an adjustable surface charge to optimize electrostatic interactions with the target pollutant. The nanostructured geometry of the porous shell—confirmed through BET and TEM analysis—plays a vital role in achieving high-performance adsorption, setting this material apart from traditional dense oxides. The adsorption behavior was significantly influenced by the pH of the solution, peaking at pH 5. The kinetics adhered to a pseudo-second-order model, and the equilibrium data fit well with the Langmuir isotherm, achieving a notable maximum adsorption capacity of 84.7 mg/g. The comprehensive parametric analysis offers essential insights for process scaling.

Furthermore, the discussion can explore the probable adsorption mechanism, which likely involves a combination of electrostatic attraction, π-π interactions between the aromatic rings of diclofenac and the Bi_2O_3 surface, along with pore-filling in the mesoporous shell. The magnetic core-shell configuration not only addresses the practical challenge of recovering nanoparticles but also paves the way for the creation of multifunctional materials—for instance, by tapping into the photocatalytic attributes of Bi_2O_3 for integrated adsorption-degradation strategies in future studies. In summary, the Fe_3O_4@Bi_2O_3 nanocomposite emerges as a highly effective, efficient, and sustainable option for addressing pharmaceutical-contaminated wastewater.

Acknowledgements

This work was made possible by the Water and Wastewater Department of Ilam Province.

References

[1] Patel, M.; Kumar, R.; Kishor, K. Pharmaceuticals of emerging concern in aquatic systems: Chemistry, occurrence, effects, and removal methods. ***Chem. Rev.*** **2019**,119 (6), 3510-3673. DOI: 10.1021/acs.chemrev.8b00299.

[2] Xu, J.; Cao, Z.; Zhang, Y.; Yuan, Z.; Lou, Z.; Xu, X.; Wang, X. A review of functionalized carbon nanotubes and graphene for heavy metal adsorption from water: Preparation, application, and mechanism. ***Chemosphere*** **2018**, 195, 351-364. DOI: 10.1016/j.chemosphere.2017.12.061.

[3] Freundlich, H. M. F. Over the adsorption in solution. ***J. Phys. Chem.*** **1906**, 57, 385-470.

[4] Ali, I.; Gupta, V. K. Advances in water treatment by adsorption technology. ***Nat. Protoc.*** **2006**, 1 (6), 2661-2667. DOI: 10.1038/nprot.2006.370.

[5] Liu, Q.; Shi, J.; Zheng, S. A review on the adsorption of heavy metals by clay minerals, with special focus on the past decade. ***Chem. Eng. J.*** **2014**, 308, 438-446. DOI: 10.1016/j.cej.2016.09.029.

[6] Richardson, S. D.; Kimura, S. Y. Water analysis: Emerging contaminants and current issues. ***Anal. Chem.*** **2016**, 88 (1), 546-582. DOI: 10.1021/acs.analchem.5b04493.

[7] Bolong, N.; Ismail, A. F.; Salim, M. R.; Matsuura, T. A review of the effects of emerging contaminants in wastewater and options for their removal. ***Desalination*** **2009**, 239 (1-3), 229-246. DOI: 10.1016/j.desal.2008.03.020.

[8] Zhang, Y.; Geißen, S. U.; Gal, C. Carbamazepine and diclofenac: Removal in wastewater treatment plants and occurrence in water bodies. ***Chemosphere*** **2008**, 73 (8), 1151-1161. DOI: 10.1016/j.chemosphere.2008.07.086.

[9] Schwaiser, J.; Ferling, H.; Mallow, U.; Wintermayr, H.; Negele, R. D. Toxic effects of the non-steroidal anti-inflammatory drug diclofenac. Part I: Histopathological alterations and bioaccumulation in fish. ***Aquat. Toxicol.*** **2004**, 68 (2), 141-150. DOI: 10.1016/j.aquatox.2004.03.014.

[10] Oaks, J. L.; Gilbert, M.; Virani, M. Z.; Watson, R. T.; Meteyer, C. U.; Rideout, B. A.; Shivaprasad, H. L.; Ahmed, S.; Iqbal Chaudhry, M. J.; Arshad, M.; Mahmood, S.; Ali, A.; Khan, A. A. Diclofenac residues as the cause of vulture population decline in Pakistan. ***Nature*** **2004**, 427 (6975), 630-633. DOI: 10.1038/nature02317.

[11] Vieno, N.; Tuhkanen, T.; Kronberg, L. Elimination of pharmaceuticals in sewage treatment plants in Finland. ***Water Res.*** **2007**, 41 (5), 1001-1012. DOI: 10.1016/j.watres.2006.12.017.

[12] Crini, G.; Lichtfouse, E. Advantages and disadvantages of techniques used for wastewater

treatment. ***Environ. Chem. Lett.*** **2019**, 17 (1), 145-155. DOI: 10.1007/s10311-018-0785-9.

[13] Lu, A. H.; Salabas, E. L.; Schüth, F. Magnetic nanoparticles: Synthesis, protection, functionalization, and application. ***Angew. Chem., Int. Ed.*** **2007**, 46 (8), 1222-1244. DOI: 10.1002/anie.200602866.

[14] Burakov, A. E.; Galunin, E. V.; Burakova, I. V.; Kucherova, A. E.; Agarwal, S.; Tkachev, A. G.; Gupta, V. K. Adsorption of heavy metals on conventional and nanostructured materials for wastewater treatment purposes: A review. ***Ecotoxicol. Environ. Saf.*** **2018**, 148, 702-712. DOI: 10.1016/j.ecoenv.2017.11.034.

[15] Ghosh, S.; Badruddoza, A. Z.; Uddin, M. S.; Hidajat, K. Adsorption of chiral aromatic amino acids onto carboxymethyl-β-cyclodextrin bonded Fe3O4/SiO2 core–shell nanoparticles. ***J. Colloid Interface Sci.*** **2011**, 354 (2), 483-492. DOI: 10.1016/j.jcis.2010.11.063.

[16] Zhang, L.; Zhu, Y. A review of controllable synthesis and enhancement of performances of bismuth tungstate visible-light-driven photocatalysts. ***Catal. Sci. Technol.*** **2009**, 2 (4), 694-706. DOI: 10.1039/B819767K.

[17] Qu, X.; Alvarez, P. J.; Li, Q. Applications of nanotechnology in water and wastewater treatment. ***Water Res.*** **2013**, 47 (12), 3931-3946. DOI: 10.1016/j.watres.2013.04.058.

[18] Savage, N.; Diallo, M. S. Nanomaterials and water purification: Opportunities and challenges. ***J. Nanopart. Res.*** **2005**, 7 (4-5), 331-342. DOI: 10.1007/s11051-005-7523-5.

[19] Liu, J.; Qiao, S. Z.; Hu, Q. H.; Lu, G. Q. Magnetic nanocomposites with mesoporous structures: synthesis and applications. ***Small*** **2011**, 7 (4), 425-443. DOI: 10.1002/smll.201001402.

[20] Hameed, A.; Montini, T.; Gombac, V.; Fornasiero, P. Surface phases and photocatalytic activity correlation of Bi2O3/Bi2O4-x nanocomposite. ***J. Am. Chem. Soc.*** **2008**, 130 (30), 9658-9659. DOI: 10.1021/ja803603y.

[21] Gupta, V. K.; Saleh, T. A. Sorption of pollutants by porous carbon, carbon nanotubes and fullerene- An overview. ***Environ. Sci. Pollut. Res***. **2013**, 20 (5), 2828-2843. DOI: 10.1007/s11356-013-1524-1.

[22] Ho, Y. S.; McKay, G. Pseudo-second order model for sorption processes. ***Process Biochem.*** **1999**, 34 (5), 451-465. DOI: 10.1016/S0032-9592(98)00112-5.

[23] Wang, S.; Peng, Y. Natural zeolites as effective adsorbents in water and wastewater treatment. ***Chem. Eng. J.*** **2010**, 156 (1), 11-24. DOI: 10.1016/j.cej.2009.10.029.

[24] Wang, X.; Li, S.; Yu, H.; Yu, J.; Liu, S. Ag_2O as a new visible-light photocatalyst: Self-stability and high photocatalytic activity. ***Chem.–Eur. J.*** **2011**, 17 (28), 7777-7780. DOI: 10.1002/chem.201101032.

[25] Huang, H.; Wang, Y.; Cai, W. A review on the morphology and material design of Bi2O3 for photocatalytic applications. ***Catal. Sci. Technol.*** **2012**, 2 (11), 2243-2253. DOI: 10.1039/C2CY20473F.